Journal of Electrical and Computer Engineering Innovations
(JECEI)
Journal homepage: http://www.jecei.sru.ac.ir

Research paper

Detailed Analysis and Design of Line-Start Synchronous Reluctance Motors Aiming at High Power Factor

Seyed Reza Mousavi-Aghdam* , ***Seyed Abbas Azimi*** , ***Farzad Sedaghati***

Department of Electrical Engineering, Faculty of Engineering, University of Mohaghegh Ardabili, Ardabil, Iran.

Article Info

Article History:
Received 23 January 2026
Reviewed 27 March 2026
Revised 16 April 2026
Accepted 23 May 2026

Keywords:
Line-start permanent magnet assisted synchronous reluctance motor
Finite element method
Line-start capability
Power factor
Efficiency

*Corresponding Author's Email Address:
r.mousaviaghdam@uma.ac.ir

Abstract

Background and Objectives: Synchronous reluctance motors (SynRMs) have considered as energy-efficient alternatives to conventional induction motors (IMs), primarily due to high efficiency. Despite their low losses, SynRMs are hindered by inadequate line-start capability and a low power factor, which restrict their use in industrial settings. This article addresses these limitations by introducing a line-start permanent magnet-assisted SynRM (LS-PMaSynRM) that incorporates fluid-type flux barriers. This design aims to enhance starting performance and increasing power factor.

Methods: The design process entailed a parametric sensitivity analysis of critical motor characteristics, including rotor geometry, stator winding configuration, and stator slot count. Finite Element Method (FEM) simulations were executed using time-stepping analysis to assess the motor's electromagnetic behavior under both transient and steady-state conditions. Performance metrics such as torque ripple, average torque, efficiency, and power factor were evaluated. Comparative simulations with conventional SynRM and PMaSynRM designs were also conducted to benchmark improvements.

Results: The proposed LS-PMaSynRM exhibited substantial enhancements in line-start capability, achieving stable synchronization within a brief period. The motor demonstrated a significant increase in power factor relative to conventional SynRM designs, while maintaining high efficiency throughout the operating range.

Conclusion: The study presents an LS-PMaSynRM architecture that effectively addresses traditional limitations in line-start performance and power factor. These findings support the broader industrial adoption of SynRMs and offer a practical design pathway for future high-efficiency motor applications.

How to cite this paper:
S. R. Mousavi-Aghdam, S. A. Azimi, F. Sedaghati, "Detailed analysis and design of line-start synchronous reluctance motors aiming at high power factor," J. Electr. Comput. Eng. Innovations, 14(2): 535-548, 2026.
DOI: 10.22061/jecei.2026.12645.899
URL: https://jecei.sru.ac.ir/article_12561.html

Introduction

Electric motor technologies are continuously undergoing improvement and exploration for commercial, agricultural, medical, and diverse industrial applications. Induction motors (IMs) are the most extensively utilized in industries due to their simple structure, line-start capability, and robustness. However, IMs exhibit limited efficiency due to copper losses, which has prompted industries to replace these prevalent electric motors with synchronous reluctance motors (SynRMs) that demonstrate higher efficiency [1], [2]. The flux barriers in the multilayer structure of the SynRM rotor decrease hysteresis and eddy current losses [3], [4]. The induced current in the rotor conductor bars remains stable at zero during synchronous operation, resulting in the absence of rotor copper losses [5]. In [6], the rotor design of the SynRM is refined by changing conventional magnetic radial ribs with non-magnetic titanium ribs. This modification decreases magnetic flux leakage along the q-axis, thereby enhancing torque, saliency ratio, efficiency, and power factor. so, this optimized rotor structure improves both electromagnetic and mechanical performance, particularly for automotive applications. Two significant challenges associated with SynRMs are low power factor and line-start capability [7], [8]. An innovative analytical modeling method for SynRMs that can substantially improve the design and analysis process of this type of machine is presented in [9]. In [10], the dynamic modeling of SynRM is examined. An accurate and efficient model to describe the dynamic behavior of SynRMs, which is crucial for their precise control is demonstrated in [10].

The introduction and analysis of a dual-stator SynRMs as a solution to decrease torque ripple in single-stator SynRMs has been proposed in [11]. The conflict between mechanical strength and magnetic performance has required the use of internal claws in the rotor [12] to enhance the power factor and torque. In [13], the effect of minor alterations in the dimensions of the SynRM rotor on the output torque of the machine is presented by providing a semi-analytical method for a rapid and accurate evaluation. This method employs a more straightforward and faster approach instead of complex and time-consuming finite element method (FEM) simulations. A suitable rotor design with a focus on flux barriers may require a fast process with constrained design flexibility [14]. This becomes even more important when a complex design, for example, a hybrid rotor with both radial and axial laminations, is considered [15]. Such methodological considerations may also be implemented for other types of reluctance motors [16]. Fast design techniques are commonly used in nonlinear systems, especially in the case of reluctance motors.

The lower power factor of SynRMs has prompted numerous researchers to add the utilization of permanent magnets (PM) in SynRMs [17], [18]. Although rare-earth PMs are costly and non-renewable, their extraction may result in significant environmental degradation if appropriate and safe measures are not implemented [19], [20]. The incorporation of PMs in the q-axis enhances the power factor of PMaSynRMs; however, it introduces substantial torque ripple [21]. The simulation and measured results for a water pump application utilizing a SynRM is presented in [22]. In [23], the dynamic performance of SynRM was optimized by filling all flux barriers with conductor bars. Based on the optimal structure of rotor flux barriers, enhancing the asynchronous torque by reducing the resistance of rotor conductor bars through increased area represents a direct and effective method for improving the synchronizing capability of line-start SynRM (LS-SynRM) [24], [25]. In [26], key design parameters of PMaSynRM were identified through sensitivity analysis, which was subsequently optimized to minimize energy loss across various driving cycles in an electric vehicle. The asymmetric rotor topologies for reducing torque ripples in SynRMs and their effect on mechanical vibration is demonstrated in [27], [28]. In [29] and [30], a comprehensive design methodology for an external and internal rotor SynRM suitable for electric bike and scooter applications are presented.

This paper presents sensitivity analyzes of SynRM with fluid-type flux barriers. It focuses on line-start capability and power factor. The efficiency improvement while maintaining a high average torque is considered. The stators of SynRMs typically possess either 24 or 36 slots, with both configurations being considered for comprehensive analysis. The design of the SynRM stator is not elaborated upon due to its resemblance to the IM stator. However, the winding configurations for both stators will be presented. Two winding configurations for 24-slot and three winding configurations for 36-slot stators are presented. stators are analyzed independently for line start capability, power factor enhancement, and additional motor parameters. The analysis process and presentation of the initial and proposed rotor design, along with stator winding specifications, are presented in the second section. The third section presents transient and steady-state results. The final section provides a comparison of both proposed LS-PMaSynRMs based on FEM results.

In conventional designs, permanent magnets are typically positioned along the q-axis. However, the proposed design introduces auxiliary magnets and auxiliary flux barriers on the d-axis, which significantly enhance the power factor and average torque of the SynRM. The effective placement of conductive bars

within the flux barriers and proximity to the q-axis facilitates the SynRM's starting without the need for additional equipment. Furthermore, the selection of the fill ratio for the bars contributes to a quicker attainment of synchronous speed and reduces aluminum consumption costs. These innovations not only improve the motor's performance but also enhance power factor, efficiency, and lower production costs, making them particularly valuable for industrial applications.

Initial Synrm Design Features

The rotor of SynRM is composed of multilayer isotropic electrical steels that are stacked in their axial direction and exhibit low magnetic reluctance. In contrast to synchronous and induction motors, which typically incorporate PM or windings in their rotor, SynRM solely contains flux barriers in its rotor. The operation of PMaSynRM is predicated on directing the magnetic fluxes generated by the stator winding currents through paths of lower reluctance within the iron paths of the rotor and stator. Consequently, the desired maximum reluctance torque can be optimized by appropriately adjusting the two predicted equivalent magnetic reluctances on the dq-axes. The stator voltage equations can be expressed as (1):

$$\begin{cases} v_{ds} = R_s i_{ds} - \omega_e \lambda_{qs} - \omega_e \lambda_{pmq} \\ v_{qs} = R_s i_{qs} + \omega_e \lambda_{ds} + \omega_e \lambda_{pmd} \end{cases} \quad (1)$$

where v_{ds}, ids, v_{qs} and i_{qs} are the stator voltage and current components on the dq-axis. ω_e is the electrical angular speed and R_s is stator winding resistance. λ_{ds} and λ_{qs} are dq-axis flux linkage, and λ_{pmd} and λ_{pmq} are dq-axis PM flux linkage, and can be expressed as (2):

$$\lambda = L_{ds} i_{ds} + \lambda_m + jL_{qs} i_{qs} \quad (2)$$

where λ_m is the flux linkage of the PMs, and L_{ds} and L_{qs} are the d-axis and q-axis components of the stator inductance. The non-saturation of the stator and rotor iron cores stabilizes these two inductance terms. The electromagnetic torque T_e of PMaSynRM is expressed by (3):

$$T_e = (\frac{3p}{4})\lambda_m i_{qs} + (\frac{3p}{4})\left(L_{ds} - L_{qs}\right) i_{ds} i_{qs} \quad (3)$$

where p is the number of poles. The difference in inductance between the d-axis and q-axis contributes to a greater torque, as explicitly demonstrated in (3). In addition to the increase in torque, the power factor of SynRMs, which is lower than that of induction motors, can be improved. However, as it is evident that PMs significantly influence the performance of PMaSynRMs, various PM combinations and manufacturing feasibility should be thoroughly evaluated during the rotor design stage. Prior to the initial design of the rotor, which is considered the most critical component in the design of SynRMs, the stator design is reviewed in its entirety.

A. Stator Winding Configuration

SynRMs can have different numbers of poles, but the most common configuration is 4 poles. In order to reduce undesirable harmonics, optimize torque production and increase efficiency in these motors, the number of stator slots is Typically 24 or 36 slots. Therefore, two stators with 24 and 36 slots are considered. The two-layer winding configuration has been selected due to its superior winding distribution in the slots, enhanced power density, improved efficiency, and increased mechanical stability. Two configurations are examined for stator winding with 24-slots, utilizing Coil Pitches (CPs) of 4 and 5. Additionally, three configurations are considered for stator winding with 36-slots, employing CPs of 6, 7, and 8, as illustrated in Fig. 1. Two SynRM designs with different stator slots are designed to validate the initial principle and performance of the proposed motor. The proposed design specifications are summarized in Table 1. Due to the similarity between the SynRM and IM stators, the stator is considered a conventional IM. Therefore, the methodology for calculating the conductor size in the

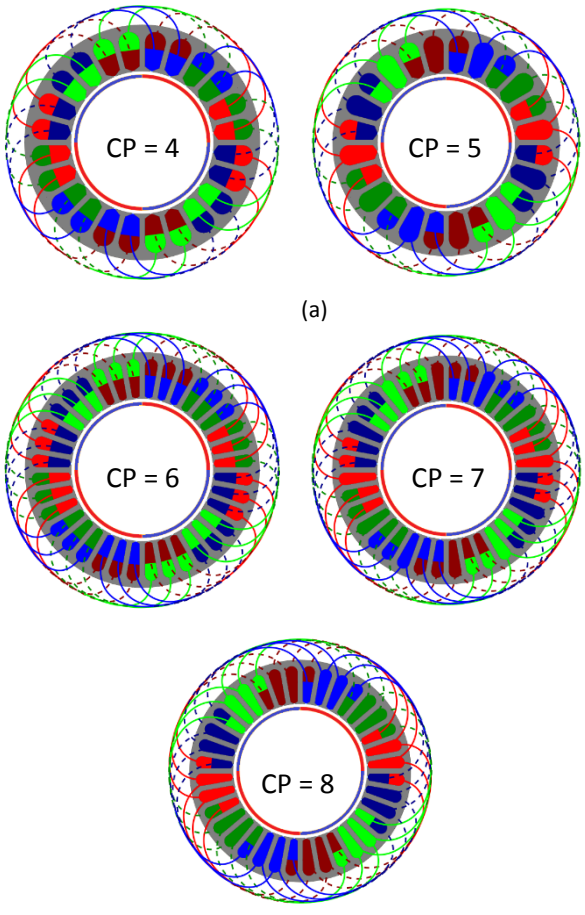

Fig. 1: Winding configuration for different CPs in SynRM with (a) 24-slot and (b) 36-slot designs.

Table 1: Main data of the proposed SynRM designs

Item	unit	value	
		24-slot	36-slot
Rated power	kW	1.5	
Rated torque	N.m	9.5	
Rated frequency	Hz	50	
Rated voltage	V	380	
Rated speed	r/min	1500	
Number of poles		4	
Winding connection		Y	
Core length	mm	86.4	66.15
Turn number of per slot		115	94
Rotor outer diameter	mm	35	40
Air gap length (mm)	mm	0.5	
Stator conductor size	mm^2	1	

SynRM stator is similar to IM. The analysis of back-EMF harmonic content reveals critical insights into the selection of coil configurations for SynRMs. The findings express the impact of stator winding on harmonic generation, emphasizing that certain CPs demonstrate superior performance in minimizing these harmonics. The stator geometry design is not considered in this paper, but it remains consistent with conventional configurations. To determine the coil for initial SynRMs, the back-EMF harmonic content for two-layer coils with possible winding pitches is presented. As illustrated in Fig. 2, the odd-order harmonic amplitude of the Back-EMF for the design with a 24-slot stator with a CP of 4 is lower than that of the other type. Additionally, in the 36-slot design, the CP of 8 exhibits superior even-order harmonic amplitude compared to the other two types. Consequently, the CP of 4 is considered for a 24-slot stator design, and the CP of 8 is considered for a 36-slot stator design.

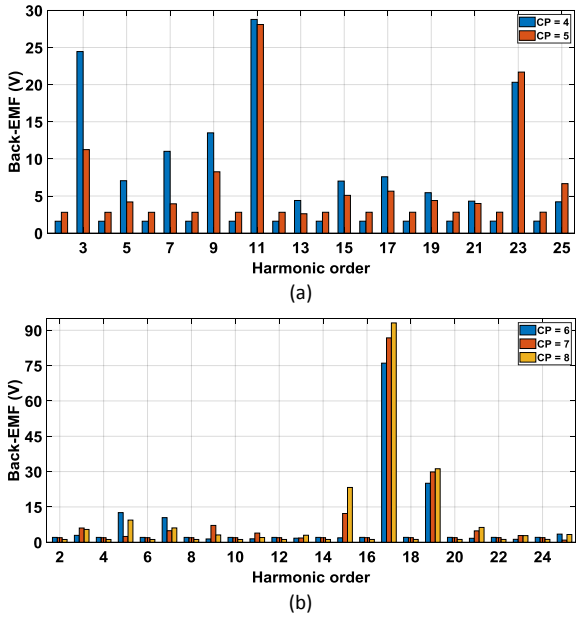

Fig. 2: The Back-EMF harmonic content of initial SynRM with (a) 24-slot and (b) 36-slot designs.

B. Parameterized Rotor design features

Fig. 3 presents the conceptual structure of a quarter of a 4-pole SynRM rotor. Flux barriers are of significant importance in rotor design; consequently, researchers have proposed various geometries, including circular, trapezoidal, segmented geometry (SEG), Salient pole, and fluid-type configurations. The fluid-type flux barrier exhibits superior torque characteristics compared to other types of flux barrier designs due to its optimized shape; consequently, fluid-type flux barriers are considered as a starting point. While the power factor of SynRM represents a significant limitation, PM usage has successfully solved this problem to some extent. It is noteworthy that the main PMs in PMaSynRM are positioned on the q-axis in accordance with (2), which consequently enhances the power factor. However, this parameter can be further optimized by strategically placing the PMs on the d-axis. PMs are typically situated within flux barriers, and the presence of these barriers ensures that the PM flux is directed in the appropriate orientation. The design of auxiliary PMs on the d-axis demands the creation of two non-magnetic gaps adjacent to the auxiliary PMs to ensure the correct direction of PM flux. Furthermore, to optimize rotor geometry and decrease demagnetization, as illustrated in Fig. 4, PMs are positioned adjacent to the shaft on the d-axis and within flux barriers on the q-axis. Fig. 5 presents the phasor diagram for the proposed PMaSynRM in comparison to the conventional SynRM. The flux linkage of PMs can be categorized into two components: the first component includes the flux linkage of PMs positioned on the d-axis ($\lambda_{m\_d\text{-}axis}$), and the second component includes the flux linkage of PMs positioned on the q-axis ($\lambda_{m\_q\text{-}axis}$).

$$\lambda_m = \lambda_{m\_d-axis} + \lambda_{m\_q-axis} \tag{4}$$

The power factor can be expressed as follows

$$\cos\phi = \frac{(L_d - L_q) i_{ds} i_{qs} + \lambda_m i_{ds}}{\sqrt{(i_{ds}^2 + i_{qs}^2)[L_d^2 i_{ds}^2 + (\lambda_m - L_q i_q)^2]}} \tag{5}$$

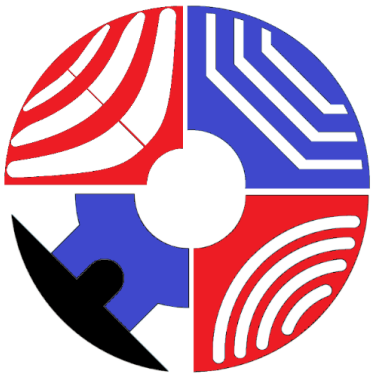

Fig. 3: The conceptual structure of a quarter of a 4-pole SynRM rotors.

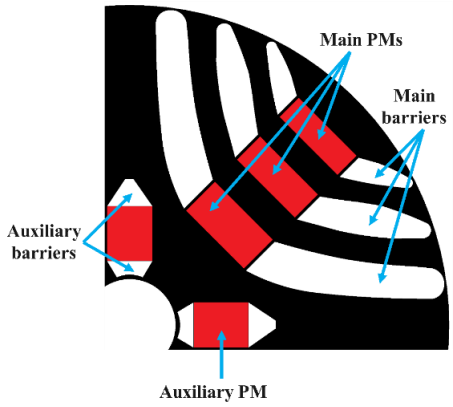

Fig. 4: The proposed modifications of the PMaSynRM design.

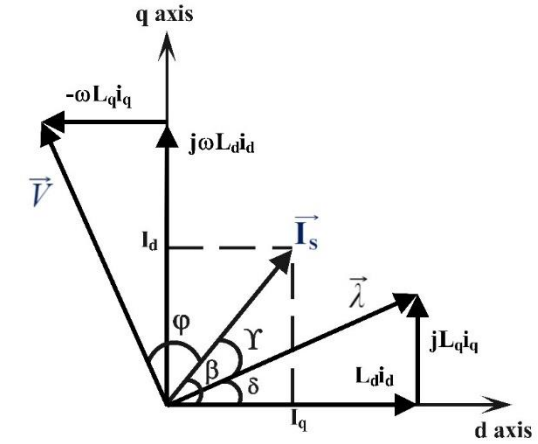

(a)

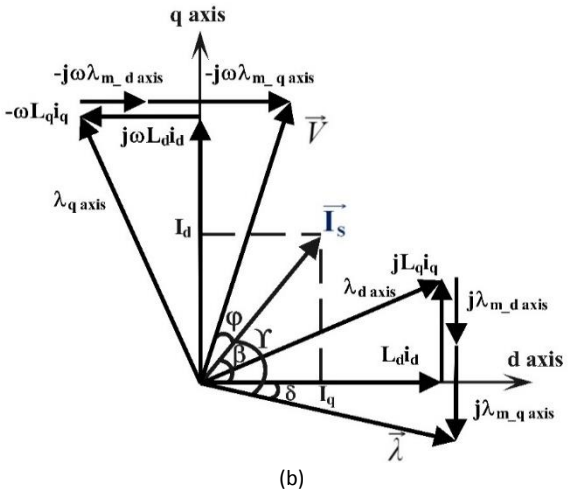

(b)

Fig. 5: Phasor diagram for the conventional (a) SynRM and, (b) The proposed PMaSynRM.

The maximum output power factor of SynRM is a function of the saliency ratio ($\zeta=L_d/L_q$).

$$\cos(\phi)_{\max} = \frac{L_d - L_q}{L_d + L_q} \tag{6}$$

The saliency ratio not only enhances the power factor but also influences the torque characteristic of the motor according to (3). Adding conductor bars in SynRMs provides line-start capability. Consequently, in this paper, the flux barriers are filled with aluminum for optimal use of space in the rotor. To prevent magnetic locking, slip, and noise, two additional flux barriers filled with aluminum are incorporated on the q-axis at each pole. The extent of aluminum infilling in the flux barriers is expressed as A_{xi}:

$$A_{xi} = r_{rotor} - (x_i . r_{rotor}) \tag{7}$$

where r_{rotor} denotes the rotor radius, and x_i represents the infilling index, which encompasses three levels: 10%, 15%, and 20%, respectively. 10% of the rotor radius is filled with aluminum inside the flux barriers in the 10% design. In the 15% and 20% designs, the flux barriers are filled with aluminum at 15% and 20% of the rotor radius, respectively. Fig. 6 together with Table 2 illustrate the design parameters and initial values for the proposed LS-PMaSynRM. The torque produced in SynRM solely is the reluctance torque (T_{rel}), which, upon the addition of a cage, results in another component being incorporated into the electromagnetic torque (T_{em}) of SynRM, termed asynchronous torque (Tasy). Consequently, in LS-SynRM, the electromagnetic torque is expressed in two components as follows:

$$T_{em} = T_{asy} + T_{rel} \sin(2s\omega t + \alpha) \tag{8}$$

where s denotes slip, ω represents the synchronous speed, and α signifies the phase angle. Fig. 7 illustrates the starting torque curve during the starting process for conventional and the proposed LS-PMaSynRM for different A_{xi}. The rotor design with %10 infilling (A10) in the conventional 24-slot design and the rotor design with %20 infilling (A20) in the conventional 36-slot design, have better starting torque than the other conventional designs. However, these two designs produce lower average torque than the proposed designs. The two rotor designs, A15 and A20, exhibit better starting performance in the proposed designs; however, the A15 design is preferred due to its lower aluminum consumption in the flux barriers. Furthermore, the A15 rotor design in the proposed designs enhanced the starting torque. Fig. 8 presents a comparison of the torque between the conventional SynRM and the proposed LS-PMaSynRM in different states, including the absence, partial, and complete presence of PMs for different current angles. As predefined, the results for both designs with 24 and 36-slot stators demonstrate that the use of auxiliary PMs generates more torque than the conventional SynRM design. The main PMs can produce more torque than auxiliary PMs, and the combination of main and auxiliary PMs yields the optimal result for torque. Ferrite PMs exhibit low remanence flux density, which may result in

demagnetization. The demagnetization of PMs can be decreased through the appropriate design of the rotor cage, as the magnetic field generated by the cage serves as a protective shield against the stator's magnetic field during starting. Fig. 9 illustrates the proposed LS-PMaSynRM designs with 24 and 36-slot stators, including their respective PM orientations. Fig. 10 illustrates the flux density of proposed designs with 24 and 36-slots at base speed. The results indicate that the PMs are not subject to irreversible demagnetization.

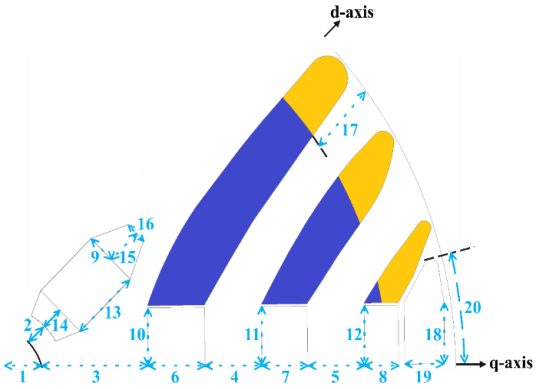

Fig. 6: Illustration of the main design parameter for the proposed PMaSynRMs (the numbers are defined in Table 2).

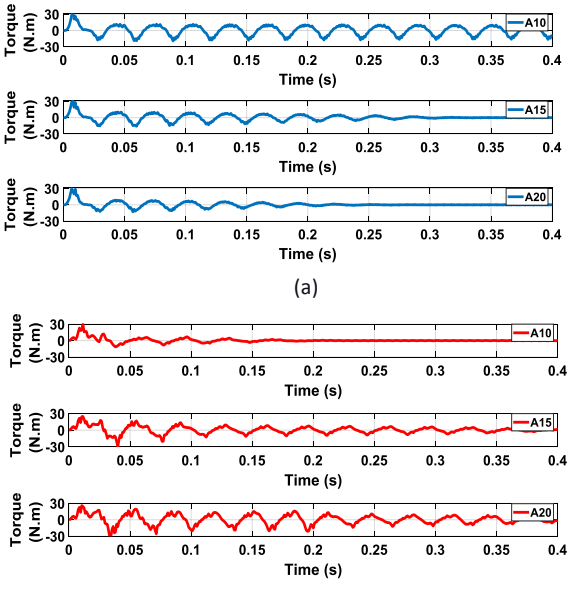

(a)

(b)

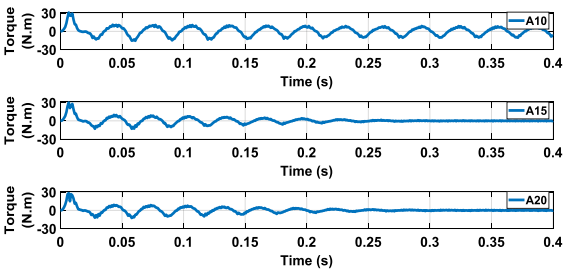

(c)

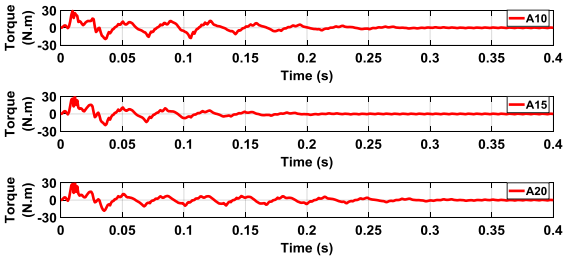

(d)

Fig. 7: Starting torque-time curves for (a) Conventional 24-slot, (b) Conventional 36-slot stator, (c) The proposed 24-slot and (d) The proposed 36-slot designs during the starting process for different A_{xi}.

Table 2: The main design parameters of the proposed LS-PMaSynRM

number	definition	Initial Value (mm)	
		24-slot	36-slot
1	Shaft diameter	5	5
2	Bridge length between the shaft and auxiliary barrier	0.5	0.5
3	Length between the shaft and main barrier	8.2	8
4	Length between the first and second main PM	3.4	5
5	Length between the second and third main PM	3	5
6	Height of first main PM	4.5	5
7	Height of the second main PM	3.6	4
8	Height of the third main PM	3	3
9	Half-height of auxiliary PM	2.5	2.5
10	Half-length of first main PM	4.5	5.3
11	Half-length of second main PM	4.5	5.3
12	Half-length of the third main PM	4.5	5.3
13	Length of auxiliary PM	6	6
14	Small gap length of the auxiliary barrier	0.5	0.5
15	Large gap length of the auxiliary barrier	5	5
16	Height the large gap of the auxiliary barrier	1	1
17	Radius of barriers infilling	A10 = 3.5 A15 = 5.25 A20 = 7	A10 = 4 A15 = 6 A20 = 8
18	Length of the middle conductor bar to q-axis	4.5	5.2
19	Height of the middle conductor bar	3	3.5
20	Middle conductor bar angle	13	13.5

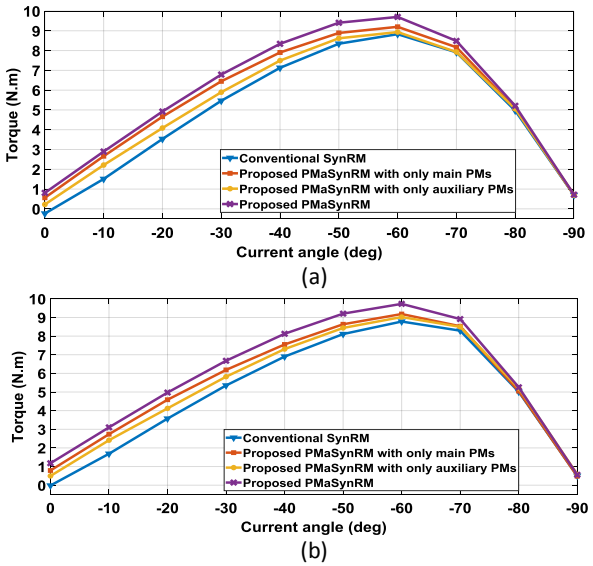

Fig. 8: Torque waveform of the conventional SynRMs and the proposed LS-PMaSynRMs in the presence or absence of different PMs in the d and q-axis for (a) 24-slot and (b) 36-slot stator designs.

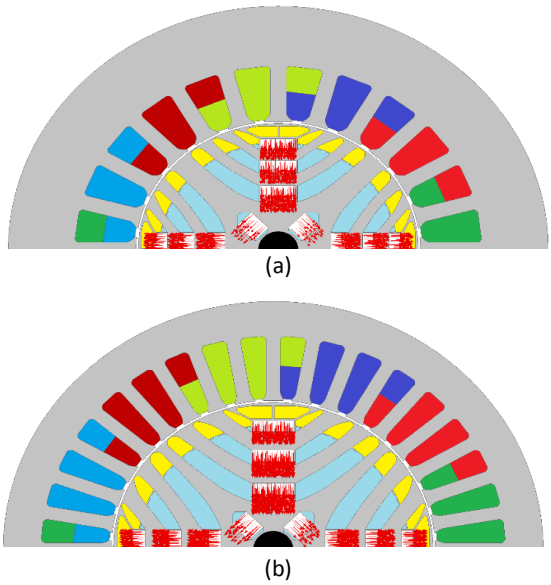

Fig. 9: Illustration of the proposed LS-PMaSynRMs and PM orientations for (a) 24-slot and (b) 36-slot designs.

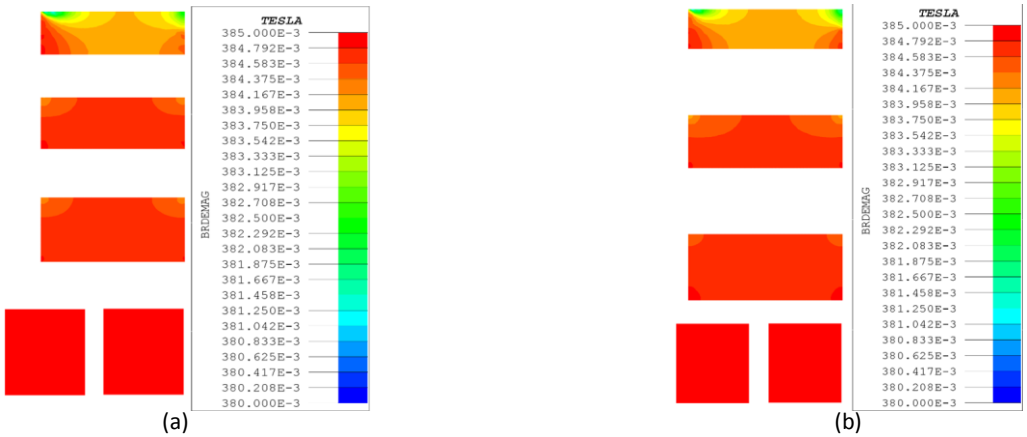

Fig. 10: Demagnetization analysis of the proposed LS-PMaSyRMs at base speed with (a) 24-slot and (b) 36-slot stator.

Performance Analysis of Proposed Design

A. Transient AC analysis

In the base speed range, the torque curve of the proposed LS-PMaSynRM exhibits an instantaneous pulse, primarily attributed to the reluctance torque. Fig. 11 depicts the torque-speed curve for both 24/36-slot stators during the starting process of conventional and the proposed LS-PMaSynRMs for different A_{xi}. In the conventional 24-slot design, A20, and the conventional 36-slot design, A10, exhibit better speed-torque characteristics. However, in the proposed design, A15, results in enhanced starting performance compared to the other designs. So, the design A15 is considered as proposed rotor design for 24-slot and 36-slot stators. proportional to the synchronization capability of the synchronous reluctance motor, with more significant inertia potentially impeding or preventing synchronization. Furthermore, in the absence of synchronization, the speed curve of the synchronous reluctance motor exhibits pulsations at twice the slip frequency, as demonstrated in (8).

The speed-time curves presented in Fig. 12 for conventional and the proposed designs, comprising 24 and 36-slots, illustrate that increase in inertia resulted in failed synchronization.

B. Steady-state Analysis

The relationship between dq-axis inductance and current for conventional and the proposed designs are shown in Fig. 13.

This demonstrates that dq-axis inductance exhibits a non-linear relationship with respect to dq-axis current. Consequently, the current significantly influences the saliency ratio.

The embedded PMs in the rotor of proposed LS-PMaSynRM results in an increased of saliency ratio compared with conventional LS-SynRMs. The Embedded of PM also enhances the torque of SynRM and increases the power factor according to (5). As illustrated in Fig. 14, the proposed LS-PMaSynRMs exhibit a higher maximum power factor.

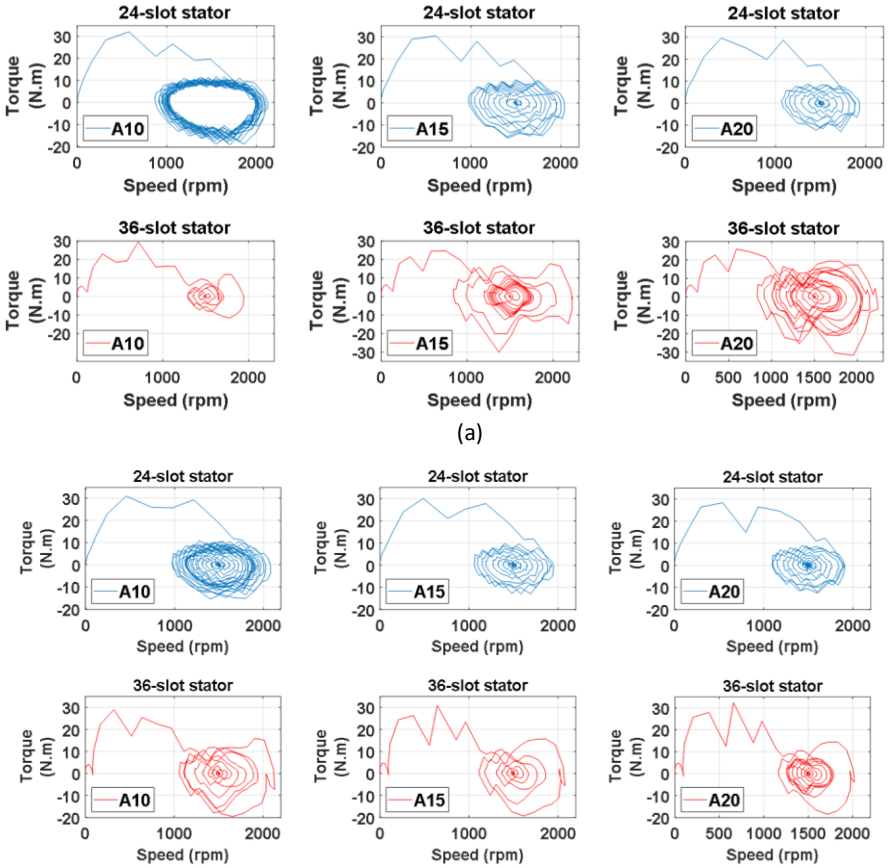

(a)

(b)

Fig. 11: The torque-speed curve for Both 24/36-slots stators during the starting process of (a) Conventional LS-SynRMs and (b) The proposed LS-PMaSynRMs in terms of different A_{xi}.

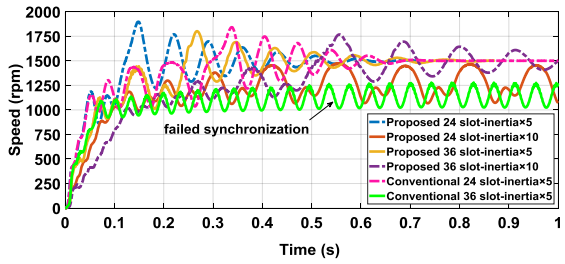

Fig. 12: Speed-time curve of conventional LS-SynRMs and the proposed Ls-PMaSynRMs in different inertia.

In Fig. 15, at low loads, the efficiency is reduced due to the fixed losses of SynRM, and with increasing load, the increase in output power decreases the effect of static losses. Ultimately, at the rated load, the efficiency reaches its maximum value, and the efficiency of the proposed LS-PMaSynRM with 24/36 stator slots exceeds that of the conventional SynRM. The power factor in terms of the current phase angle for conventional and the proposed LS-PMaSynRMs is presented in Fig. 16. As shown, embedding PMs in both proposed designs has resulted in an increased power factor. The stator and rotor, electrical steel M400-50A is utilized. The magnetic flux density of conventional and the proposed topologies is presented in Fig. 17. Additionally, the vector potential is depicted in the form of isolines. The stator yoke of topologies, under-rated current loading, experiences a flux density of less than 2 T, which falls within the normal range and does not adversely affect motor performance. The air gap magnetic flux density distribution with spatial harmonic content of conventional and the proposed LS-PMaSynRMs with 24 and 36-slot stators, analyzed using finite element analysis (FEA), is illustrated in Fig. 18. The fundamental, 3rd, 5th, up to 30th harmonic contents are depicted. The proposed 24-slot design demonstrates effective electromagnetic torque production when compared to conventional 24-slot design.

C. Mechanical stress Analysis

In the analysis of mechanical stress, centrifugal forces resulting from a rotational speed of 750 and 1500 rpm were applied. As illustrated in Fig. 19, the maximum von Mises stress observed in the proposed designs is less than that in conventional designs. The maximum von Mises stress calculated for 24-slot in nominal speed was about 2.7 MPa, while for 36-slot it was about 4 MPa. These values indicate that the rotor remains within the safe operating range, and the structural design of the rotor satisfies the mechanical strength requirements.

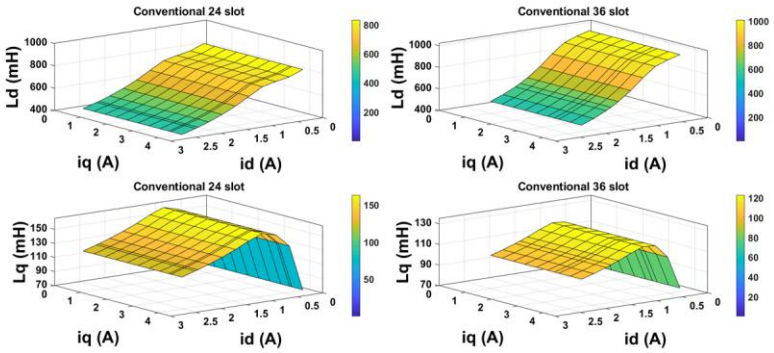

(a)

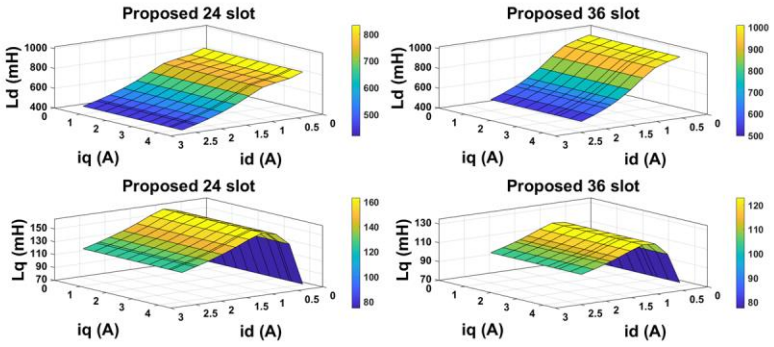

(b)

Fig. 13: The variation trend of dq-axis inductance with the current of (a) Conventional LS-SynRMs and (b) The proposed LS-PMaSynRMs.

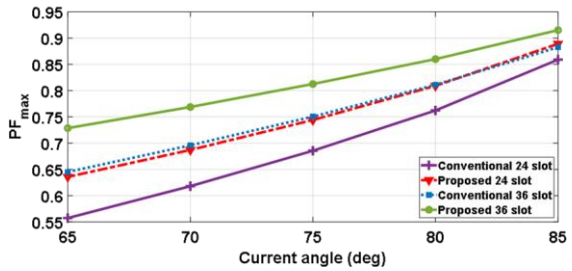

Fig. 14: The maximum power factor of conventional LS-SynRMs and the proposed LS-PMaSynRMs.

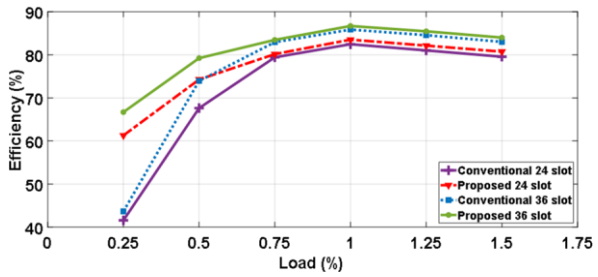

Fig. 15: Calculated efficiency of conventional LS-SynRMs and the proposed LS-PMaSynRMs.

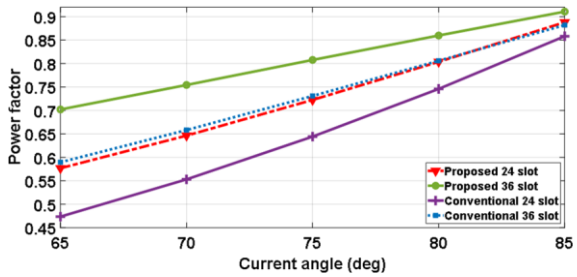

Fig. 16: Power factor of conventional LS-SynRMs and the proposed LS-PMaSynRMs.

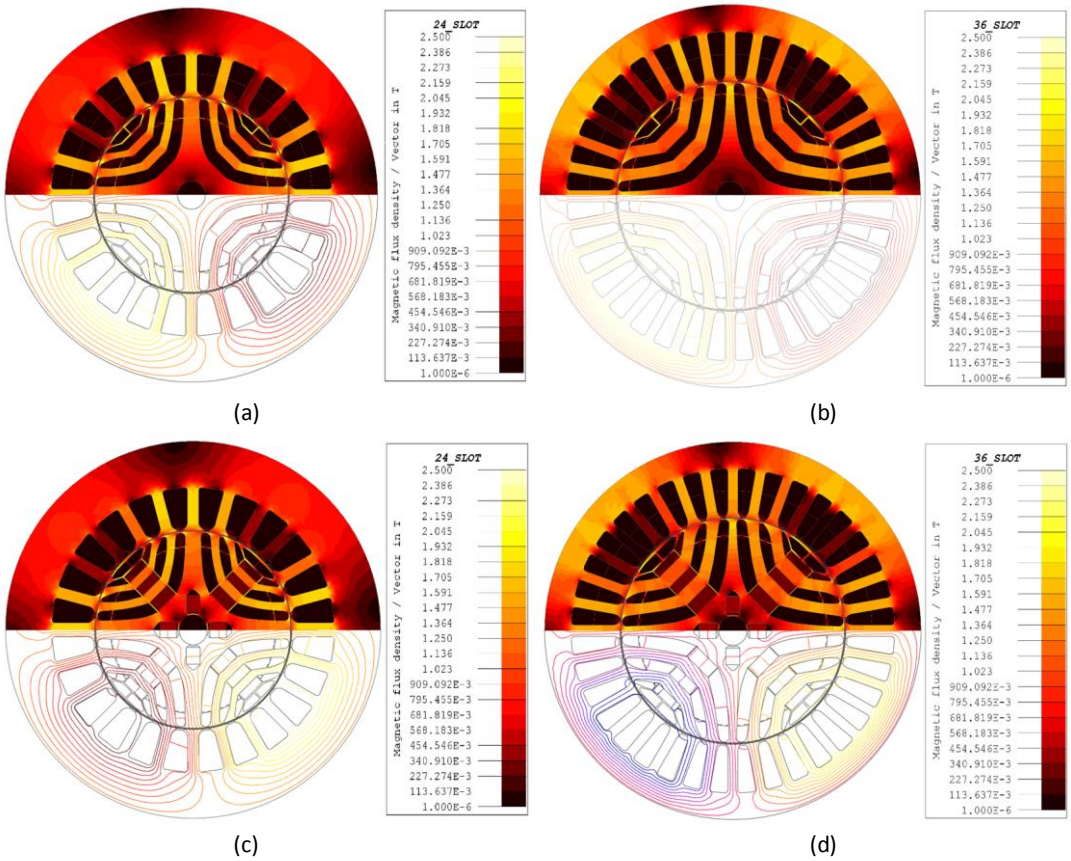

Fig. 17: The magnetic flux density and flux lines of (a) Conventional 24-slot LS-SynRM, (b) Conventional 36-slot LS-SynRM, (c) The proposed 24-slot LS-PMaSynRMs and (d) The proposed 3-slot LS-PMaSynRMs.

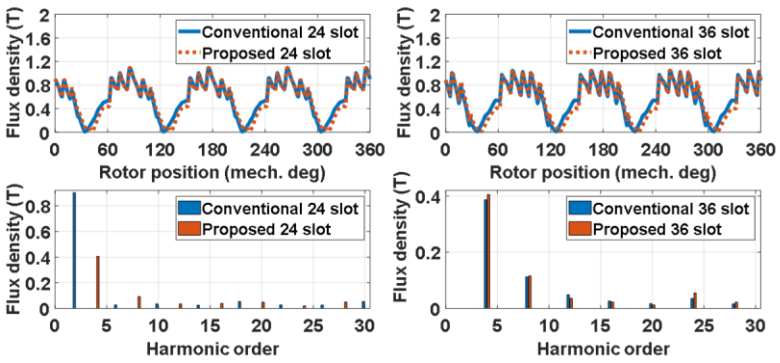

Fig. 18: The air gap magnetic flux density distribution with spatial harmonic content of conventional LS-SynRMs and the proposed LS-PMaSynRMs.

Experimental Verifications Comparisons

The proposed design with 24 stator slots has been constructed to verify the experimental results. Comparison of the Back-EMF waveforms for conventional, proposed 24-slot stator design and experimental proposed 24-slot stator design is shown in Fig. 20, wherein the waveform of the proposed 24-slot design exhibits a more sinusoidal compared to the 36-slot design.

Table 3 presents the power factor$_{max}$, power factor, efficiency, and rated current of the two proposed LS-PMaSynRM. The results under nominal conditions demonstrate that in the 24-slot design, the efficiency of the 24-slot design has increased by 1.2% from 82.5% for SynRM to 83.5% in the proposed design. In the 36-slot design, the efficiency has increased by 1% from 85.8% for SynRM to 86.7% in the proposed design. The maximum power factor and power factor for the proposed 24-slot design are 0.84 and 0.83, respectively, while for the proposed 36-slot design, they are 0.88 and 0.87, respectively.

The maximum mechanical stress for the proposed 24-slos is 2.74 MPa, and for the proposed 36-slot, it is 4 MPa. The rotor and stator stakes for the proposed 24-slot stator are depicted in Fig. 21.

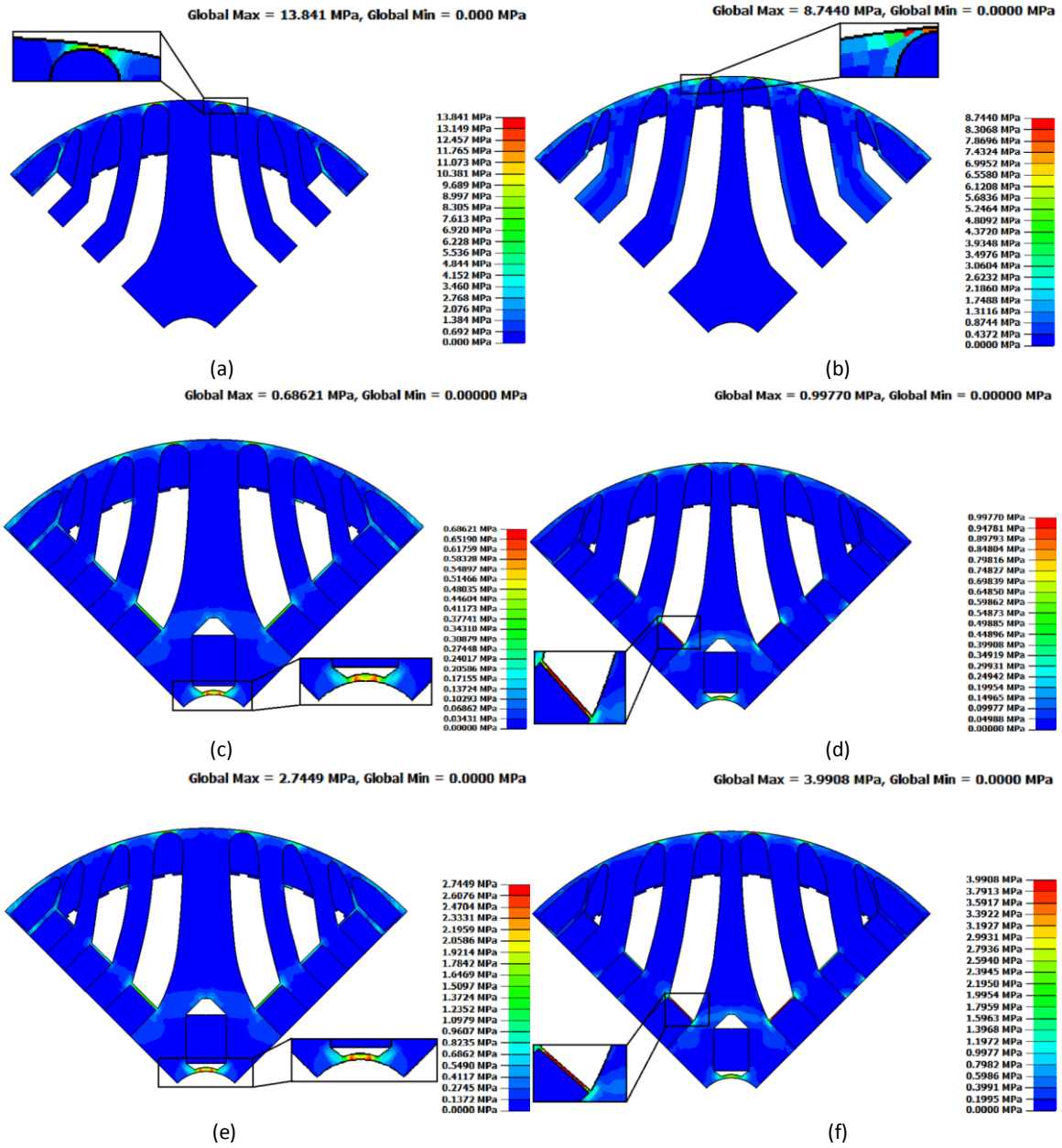

Fig. 19: Von Mises stress plot of (a) Conventional rotor design with 24-slot, (b) Conventional rotor design with 36-slot, (c) The proposed rotor design with 24-slot (rotational speed of 750 rpm), (d) The proposed rotor design with 36-slot (rotational speed of 750 rpm) (e) The proposed rotor design with 24-slot (rotational speed of 1500 rpm) and (f) The proposed rotor design with 36-slot (rotational speed of 1500 rpm).

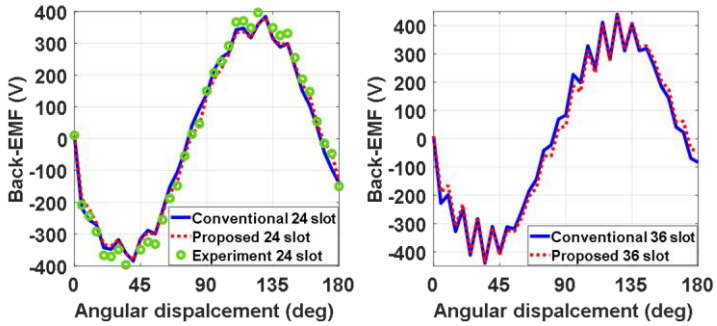

Fig. 20: Back-EMF waveforms comparison at 1500 r/min for conventional LS-SynRMs, the proposed LS-PMaSynRMs and experimental 24-slot stator LS-PMaSynRM.

Table 3: Results for both proposed LS-PMaSynRMs

Item	24-slot stator	36-slot stator
Power factor$_{max}$	0.84	0.88
Power factor	0.83	0.87
Efficiency (%)	83.5	86.7
Reted current (A)	4.4	3.8
Maximum mechanical stress (MPa)	2.74	4

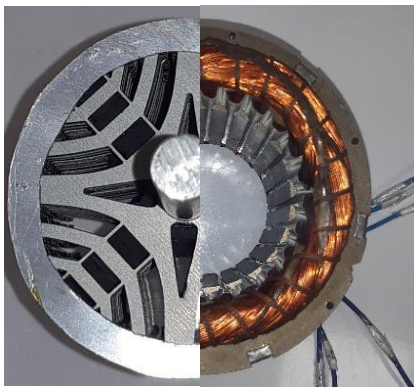

Fig. 21: Prototype of the proposed LS-PMaSynRM with 24-slot stator and rotor.

To validate the FEM analysis, the back-EMF waveform of the proposed design was measured and compared with the FE simulation results. The experimental findings confirm the performance of the proposed design.

The results for both proposed LS-PMaSynRM designs demonstrate enhanced performance compared to conventional LS-SynRMs, indicating that the proposed designs are potentially suitable for industrial and domestic applications. Industries such as mining, steel production, and chemical processing can benefit from the proposed LS-PMaSynRM. By providing enhanced efficiency and reduced losses, the proposed LS-PMaSynRMs not only meet the operational demands of these industries but also contribute to sustainability goals by lowering energy consumption and minimizing waste.

Conclusion

This study presents the design and analysis of a novel LS-PMaSynRM with fluid-type flux barriers. The analysis focuses on designing a SynRM that possesses line-start capability, improved power factor, and enhanced overall efficiency. The stator winding design incorporates two-layer windings to minimize harmonic content and enhance performance. The rotor design integrates fluid-type flux barriers with strategically placed PMs on both the q-axis and d-axis to enhance power factor and torque characteristics. A sensitivity analysis was conducted to determine the proper infill level of aluminum in the flux barriers, considering factors such as starting torque and aluminum consumption. The results demonstrate that an infill level of 15% (A15) provides the proper balance between starting performance and material utilization.

FEA was employed to calculate the motor's electromagnetic performance, including torque characteristics, power factor, and flux density distribution.

The proposed design with 24-slots demonstrates a power factor of 0.83, an efficiency of 83.5%, and a maximum mechanical stress of 2.74 MPa and the proposed design with 36-slot exhibits a power factor of 0.87, an efficiency of 86.7%, and a maximum mechanical stress of 4 MPa. The analysis indicates that the PMs are not susceptible to demagnetization under normal operating conditions. The proposed designs capabilities make them ideal for applications where reliable starting and high efficiency are paramount, such as in conveyor systems, pumps, and fans within manufacturing facilities. In conclusion, this research presents a novel and promising design for LS-PMaSynRMs with enhanced performance characteristics.

The proposed design demonstrates the potential for improved efficiency, reduced losses, High mechanical strength and enhanced reliability in various industrial applications.

Author Contributions

S. R. Mousavi-aghdam: Resources, project administration, funding acquisition, supervision, Methodology. S. A. Azimi: software, writing—review & editing, visualization, project administration, Validation. F. Sedaghati: supervision, Validation, Methodology.

Acknowledgment

We appreciate the referees and their colleagues who helped the authors in publishing this article.

Funding

This research received no external funding.

Conflict of Interest

The authors declare no potential conflict of interest regarding the publication of this work. In addition, the ethical issues including plagiarism, informed consent, misconduct, data fabrication and, or falsification, double publication and, or submission, and redundancy have been completely witnessed by the authors.

Abbreviations

SynRM	Synchronous reluctance motor
IM	Induction motor
FEM	Finite element method
SEG	Segmented geometry
CP	Coil Pitch
T_{rel}	Reluctance torque
T_{em}	Electromagnetic torque
T_{asy}	Asynchronous torque
PM	Permanent magnet

References

[1] X. Li, Y. Wang, Y. Cheng, D. Li, R. Qu, "An overview of high-efficiency synchronous reluctance machines," CES Trans. Electr. Mach. Syst., 7(1): 81–91, 2023.

[2] M. Gamba, E. Armando, G. Pellegrino, A. Vagati, B. Janjic, J. Schaab, "Line-start synchronous reluctance motors: Design guidelines and testing via active inertia emulation," in Proc. 2015 IEEE Energy Conversion Congress and Exposition (ECCE): 4820–4827, 2015.

[3] G. A. Uvaraj, N. C. Lenin, S. Padmanaban, B. Khan, "Line start synchronous reluctance motor with improved power factor for agriculture electric pump applications," J. Eng., 2022(3): 295–310, 2022.

[4] Y. Kong, B. Nicola, M. Lin, "Loss functions and efficiency model of permanent magnet assisted synchronous reluctance machine," IEEE Trans. Energy Convers., 38(1): 53–63, 2023.

[5] M. Farhadian, M. Moallem, B. Fahimi, B. M. Dehkordi, M. Sahebzamani, "Alternate rotor design for line-start synchronous reluctance motor with minimum use of copper," IEEE Access, 12: 73–84, 2024.

[6] S. Panda, R. K. Keshri, A. Tessarolo, G. Tiwari, M. Mezzarobba, "Design refinements of synchronous reluctance motor utilising non-magnetic radial ribs for traction applications," IET Electr. Power Appl., 14(2): 2480–2489, 2020.

[7] M. Muteba, "Line-Start synchronous reluctance motor with v-shaped rotor laminations," IEEE Access, 10: 109277–109288, 2022.

[8] H. Kim et al., "Study on analysis and design of line-start synchronous reluctance motor considering rotor slot opening and bridges," IEEE Trans. Magn., 58(2): 1–6, 2022.

[9] M. U. Naseer, A. Kallaste, B. Asad, T. Vaimann, A. Rassõlkin, "Analytical modelling of synchronous reluctance motor including non-linear magnetic condition," IET Electr. Power Appl., 16(4): 511–524, 2022.

[10] L. Ren, H. Wang, S. Ren, Z. Zhong, F. Peng, Y. Zhao, "Dynamic characterization of SynRM with dual-axis hybrid excitation self-commissioning," IEEE Trans. Ind. Electron., 71(5): 4440–4449, 2024.

[11] A. Mahmoudi, E. Roshandel, S. Kahourzade, W. L. Soong, "Introduction of double-stator synchronous reluctance motor and modeling," IEEE Access, 11: 76739–76750, 2023.

[12] R. Rouhani, S. E. Abdollahi, S. A. Gholamian, "Design of a high speed interior claw synchronous reluctance machine," Int. Trans. Electr. Energy Syst., 31(12): e13200, 2021.

[13] C. Madariaga, C. Gallardo, J. A. Tapia, W. Jara, A. Escobar, M. Degano, "Fast assessment of rotor barrier dimensional allowances in synchronous reluctance machines," IEEE Access, 11: 58349–58358, 2023.

[14] W. J. Wan, Z. C. Li, J. P. Lu, Y. Wang, D. Shi, J. X. Shen, "Fast design methodology for synchronous reluctance machine rotor with circular flux barriers," IEEE Trans. Ind. Appl., 61(5): 6951-6961, 2025.

[15] R. Rouhani, S. Abdollahi, A. Gholamian, "Design of a synchronous reluctance motor with new hybrid lamination rotor structure," J. Electr. Comput. Eng. Innovations, 11(2): 243-252, 2023.

[16] S. R. Mousavi-Aghdam, M. R. Feyzi, N. Bianchi, M. Morandin, "Design and analysis of a novel high-torque stator-segmented SRM," IEEE Trans. Ind. Electron., 63(3): 1458–1466, 2016.

[17] A. Jamali-Fard, M. Mirsalim, "Design and prototyping of a novel line-start permanent magnet assisted synchronous reluctance motor for fan application," IEEE Trans. Energy Convers., 39(1): 243–251, 2024.

[18] S. M. Mousavi Bafrouei, A. D. Aliabad, E. Amiri, "Design and analysis of PM-assisted synchronous reluctance machine with shifted magnetic poles," IET Electr. Power Appl., 18(1): 52–63, 2024.

[19] C. Diao, W. Zhao, Y. Liu, X. Wang, "Permanent magnet assisted synchronous reluctance motor with asymmetric rotor for high torque performance," CES Trans. Electr. Mach. Syst., 7(2): 179–186, 2023.

[20] E. Eser, N. Üstkoyuncu, "Effects of permanent magnets on different flux barriers for the AF-SynRMs," Electr. Power Compon. Syst., 52(10): 1936–1945, 2024.

[21] T. Mohanarajah, M. Nagrial, J. Rizk, A. Hellany, "a novel method to optimize permanent magnet assisted synchronous reluctance machines," Electr. Power Compon. Syst., 48(9–10): 933–943, 2020.

[22] S. Baka, S. Sashidhar, B. G. Fernandes, "Design of an energy efficient line-start two-pole ferrite assisted synchronous reluctance motor for water pumps," IEEE Trans. Energy Convers., 36(2): 961–970, 2021.

[23] C. T. Liu, et al., "Structural optimizations of high-efficiency direct-on-line synchronous reluctance motors for metal industry applications," IEEE Trans. Ind. Appl., 57(3): 3004–3011, 2021.

[24] Y. Hu, B. Chen, Y. Xiao, J. Shi, X. Li, L. Li, "Rotor design and optimization of a three-phase line-start synchronous reluctance motor," IEEE Trans. Ind. Appl., 57(2): 1365–1374, 2021.

[25] S. R. Mousavi-Aghdam, A. Azimi, "Design and analysis of a new improved rotor structure in line-start synchronous reluctance motors," Electr. Eng., 106(3): 2313–2324, 2024.

[26] L. Shao, D. Tavernini, A. E. Hartavi Karci, A. Sorniotti, "Design and optimisation of energy-efficient PM-assisted synchronous reluctance machines for electric vehicles," IET Electr. Power Appl., 17(6): 788–801, 2023.

[27] Y. Lin, Y. Sun, Y. Wang, S. Cai, J. Shen, "Radial electromagnetic force and vibration in synchronous reluctance motors with asymmetric rotor structures," IET Electr. Power Appl., 15(9): 1125–1137, 2021.

[28] Y. Zheng, et al., "A torque ripple reduction method for the synchronous reluctance machines with mirror asymmetric rotor laminations," IEEE Trans. Ind. Electron., 72(10): 10497-10507, 2025.

[29] H. Aghazadeh, E. Afjei, A. Siadatan, "Sizing and detailed design procedure of external rotor synchronous reluctance machine," IET Electr. Power Appl., 13(8): 1105–1113, 2019.

[30] S. R. Salehinia, S. E. Afjei, A. Hekmati, "Analytical method for optimal design of synchronous reluctance motor for electric scooter application," Sci. Iran., 29(5): 2537-2551, 2022.

Biographies

Seyed Reza Mousavi-Aghdam received his M.Sc. and Ph.D. Degree from University of Tabriz, Iran, in 2011 and 2015 respectively all in Electrical Engineering. During September 2014 to March 2015, he has been a Visiting Research Scholar at the Department of Industrial Engineering, University of Padova, Italy. In 2016, he joined the Department of Electrical Engineering, University of Mohaghegh Ardabili, as an Assistant Professor. Since 2020, he has been an Associate Professor of Electrical Engineering. His activity deals with the design and control of electrical machines using FEM, electric drives and converters. He is the author or coauthor of several scientific papers on electrical machines and drives. His current research interests include design and control of electrical machines and electric drives.

- Email: r.mousaviaghdam@uma.ac.ir
- ORCID: 0000-0002-0154-4427
- Web of Science Researcher ID: NA
- Scopus Author ID: 355001780700

Homepage:
https://academics.uma.ac.ir/profiles?Name=S.%20R.%20Mousavi-Aghdam

Seyed Abbas Azimi was born in Ardabil, Iran, on February, 1996. He received his B.Sc. degree in Electrical Engineering from Islamic Azad University, Ardabil branch, Ardabil, Iran in 2018 and his M.Sc. degree in Power Electronics and electric machines engineering from the Azarbaijan Shahid Madani University, Tabriz, Iran in 2021. he is currently pursuing the Ph.D. degree in the Electrical Engineering at University of Mohaghegh Ardabili in Ardabil, Iran. His research interests include electric vehicle and power electronics design, simulation, modeling, and control of electrical machines.

- Email: abbasazimi@uma.ac.ir
- ORCID: 0009-0004-4886-2213
- Web of Science Researcher ID: NA
- Scopus Author ID: 58975611100
- Homepage: NA

Farzad Sedaghati was born in Ardabil, Iran, in 1984. He received the M.S. and Ph.D. degrees both in Electrical Engineering in 2010 and 2014 from the University of Tabriz, Tabriz, Iran. In 2014, he joined the Faculty of Engineering, Mohaghegh Ardabili University, where he has been an Assistant Professor, since 2014. His current research interests include renewable energies and power electronic converters design and applications.

- Email: farzad.sedaghati@uma.ac.ir
- ORCID: 0000-0001-6974-4719
- Web of Science Researcher ID: NA
- Scopus Author ID: 35410298600
- Homepage: https://academics.uma.ac.ir/profiles?Id=617